Monthly Notices of the ROYAL ASTRONOMICAL SOCIETY

MNRAS **474,** 2594–2606 (2018) doi:10.1093/mnras/stx2935
Advance Access publication 2017 November 14

The Illustris simulation: supermassive black hole–galaxy connection beyond the bulge

Burçin Mutlu-Pakdil,[1,2,3]★ Marc S. Seigar,[1] Ian B. Hewitt,[4] Patrick Treuthardt,[4] Joel C. Berrier[5] and Lauren E. Koval[6]

[1]*Department of Physics and Astronomy, University of Minnesota Duluth, 1023 University Drive, Duluth, MN 55812-3009, USA*
[2]*Minnesota Institute for Astrophysics, University of Minnesota Twin Cities, 106 Pleasant St SE, Minneapolis, MN 55455, USA*
[3]*Department of Astronomy and Steward Observatory, 933 North Cherry Avenue, Rm. N204, Tucson, AZ 85721-0065, USA*
[4]*Astronomy and Astrophysics Research Laboratory, North Carolina Museum of Natural Sciences, 11 W. Jones Street, Raleigh, NC 27601, USA*
[5]*Department of Physics and Astronomy, The University of Nebraska at Kearney, 2504 9th Ave., Kearney, NE 68849, USA*
[6]*Department of Physics and Astronomy, Oberlin College, 110 N. Professor Street, Oberlin, OH 477074, USA*

Accepted 2017 November 10. Received 2017 November 9; in original form 2017 April 4

ABSTRACT

We study the spiral arm morphology of a sample of the local spiral galaxies in the Illustris simulation and explore the supermassive black hole–galaxy connection beyond the bulge (e.g. spiral arm pitch angle, total stellar mass, dark matter mass, and total halo mass), finding good agreement with other theoretical studies and observational constraints. It is important to study the properties of supermassive black holes and their host galaxies through both observations and simulations and compare their results in order to understand their physics and formative histories. We find that Illustris prediction for supermassive black hole mass relative to pitch angle is in rather good agreement with observations and that barred and non-barred galaxies follow similar scaling relations. Our work shows that Illustris presents very tight correlations between supermassive black hole mass and large-scale properties of the host galaxy, not only for early-type galaxies but also for low-mass, blue and star-forming galaxies. These tight relations beyond the bulge suggest that halo properties determine those of a disc galaxy and its supermassive black hole.

Key words: methods: numerical – Galaxy: formation – galaxies: spiral – cosmology: theory.

1 INTRODUCTION

It is now well accepted that supermassive black holes (BHs) reside at the centre of most massive galaxies, both quiescent and active (Kormendy & Richstone 1995; Magorrian et al. 1998; Barth 2004; Kormendy 2004). In the last decades, several scaling relationships between the mass of the central BH and the overall morphology and dynamics of the host galaxy have been found and pointed to a co-evolution scenario of galaxy formation and BH growth. Some of these properties, known to correlate well with the BH mass, are spheroid velocity dispersion ($\sigma_{\rm sph}$; e.g. Ferrarese & Merritt 2000; Gebhardt et al. 2000; Tremaine et al. 2002; Gültekin et al. 2009; McConnell & Ma 2013), spheroid luminosity ($L_{\rm sph}$; e.g. Kormendy & Richstone 1995; Graham 2007; Graham & Scott 2013), spheroid stellar mass ($M_{\rm sph}$; e.g. Kormendy & Richstone 1995; Magorrian et al. 1998; Häring & Rix 2004; Savorgnan 2016), the central stellar concentration of the spheroid (Graham et al. 2001), Sérsic index (n) of the major-axis surface brightness profile (e.g. Graham et al. 2003; Graham & Driver 2007; Savorgnan et al. 2013), and spiral arm pitch angle (P: a measure of the tightness of spiral arms; Seigar et al. 2008; Berrier et al. 2013). A common interpretation for these relationships is that BHs regulate their own growth and that of their host galaxies through active galactic nucleus (AGN) feedback (Silk & Rees 1998; Springel, Di Matteo & Hernquist 2005; Bower et al. 2006; Croton et al. 2006; Di Matteo et al. 2008; Ciotti, Ostriker & Proga 2009; Fanidakis et al. 2011). Therefore, these scaling relations have important implications not only for BHs and galaxies but also for understanding the effects of AGN feedback.

Recent observational studies have significantly revised these scaling relations, and reported that galaxies with different properties (e.g. pseudo-bulges versus real bulges, barred versus non-barred, or cored versus power-law ellipticals) may correlate differently with their central BH masses (e.g. Graham 2008; Gebhardt et al. 2011; Kormendy & Ho 2013; McConnell & Ma 2013). Therefore, it is of fundamental importance to investigate the supermassive BH–galaxy connection from a theoretical point of view and also investigate if supermassive BH–galaxy co-evolution occurs for all galaxy types or if different galaxy types hold weaker or stronger

★ E-mail: bmutlupakdil@as.arizona.edu

physical links with their BHs. Although several cosmological simulations have investigated the supermassive BH–galaxy connection and confirmed the establishment of the scaling relations (e.g. Sijacki et al. 2007; Di Matteo et al. 2008; Booth & Schaye 2009; Dubois et al. 2012; Hirschmann et al. 2014; Khandai et al. 2015; Schaye et al. 2015), the co-evolution of the BHs and their galaxies in different galaxy types has not been studied in detail. This is due to the difficulty in simulating representative galaxy samples with significant spatial resolution. Recently, the Illustris simulation project (e.g. Genel et al. 2014; Vogelsberger et al. 2014) has successfully simulated representative galaxy samples covering the observed range of morphologies and provided good spatial resolution to resolve the basic structural properties of the host galaxies. This has made it possible to study the supermassive BH–galaxy connection in detail.

Illustris is a large-scale and high-resolution hydrodynamic simulation, with a broad range of astrophysical processes: gas cooling with radiative self-shielding corrections, energetic feedback from growing BHs and exploding supernovae, stellar evolution and associated chemical enrichment and stellar mass loss, and radiation proximity effects for AGN (see Vogelsberger et al. 2014, for details). By using a small subset of 42 spiral galaxies, Vogelsberger et al. (2014) demonstrated that Illustris reproduces the observed stellar and baryonic Tully–Fisher relation (Tully & Fisher 1977; McGaugh 2012) reasonably well. Sijacki et al. (2015) presented results on the BH scaling relations relative to bulge ($M_{\rm sph}$ and $\sigma_{\rm sph}$) from the Illustris simulation. They concluded that BHs and galaxies co-evolve at the massive end, but there is no tight relation with their central BH masses for low-mass, blue and star-forming galaxies. Here, we study the BH scaling relations beyond the bulge, i.e. spiral arm pitch angle, total stellar mass ($M_{\star,\,\rm total}$), dark matter (DM) mass ($M_{\rm DM}$), and total halo mass ($M_{\rm halo}$) to complement the study of Sijacki et al. (2015). We compare the Illustris predictions with other theoretical results and observational constraints to further understanding of the supermassive BH–galaxy connection. To do so, we first concentrate on a randomly selected sample of the Illustris spiral galaxies that do not have rings, and study the face-on spiral arm morphology in multiple wavebands (*B*, *R*, and *K*). We explore its connection with BH and DM for our sample of spiral galaxies in Illustris. Then, we focus on the redshift $z = 0$ central galaxies with $10.0 < \log(M_{\star,\,2R}/{\rm M}_\odot) < 13.0$, where $M_{\star,\,2R}$ is the stellar mass within the 2 × stellar half-mass radius, and study the Illustris predictions relative to the $M_{*,\,\rm total}$, $M_{\rm DM}$, and $M_{\rm halo}$ of the host galaxy. Note that Snyder et al. (2015) presented the Illustris predictions of the $M_{\rm BH}$–$M_{*,\,\rm total}$ and $M_{\rm BH}$–$M_{\rm DM}$ relationships in the context of their implications for galaxy morphology. They investigated how Illustris galaxy morphologies depend on other aspects of the simulated galaxies, such as their optical sizes, BH masses, and DM halo masses. However, our aim is to first clearly understand these different relations (e.g. which one may be the strongest correlation), especially for low-mass, blue and star-forming galaxies.

This paper is organized as follows. In Section 2 we concentrate on a sample of the simulated spiral galaxies to study the spiral arm morphology in multiwavebands (Section 2.1) and explore its connection with the BH and DM masses (Section 2.2). In Section 3 we study the Illustris predictions relative to the $M_{*,\,\rm total}$ (Section 3.1), $M_{\rm DM}$ (Section 3.2), and $M_{\rm halo}$ (Section 3.3) of the host galaxies by comparing with other theoretical results and observational constraints. We finally discuss our results and draw conclusions in Section 4.

2 THE ILLUSTRIS SPIRAL ARM MORPHOLOGY AND PITCH ANGLE SCALING RELATIONS

2.1 Spiral arm morphology in multiwavebands

The Illustris project consists of hydrodynamical simulations of galaxy formation in a box of 75 Mpc h^{-1} (=106.5 Mpc) on the side (Genel et al. 2014; Vogelsberger et al. 2014). This volume was simulated with and without baryons at several resolution levels, here we present results from the simulation with the highest resolution (with $N_{\rm DM} = 1820^3$ DM particles and $N_{\rm baryon} = 1820^3$ baryon resolution elements) that resolves baryonic matter with mass $1.26 \times 10^6\,{\rm M}_\odot$. For all calculations, we adopt the cosmology used for the Illustris simulation, that is cosmological parameters consistent with the latest *Wilkinson Microwave Anisotropy Probe* (*WMAP*)-9 measurements ($\Omega_{\rm M} = 0.2726$, $\Omega_\lambda = 0.7274$, $\Omega_{\rm b} = 0.0456$, $\sigma_8 = 0.809$, and $H_0 = 70.4\,{\rm km\,s^{-1}\,Mpc^{-1}}$ with $h = 0.704$). Parameters in Illustris were tuned to match the redshift $z = 0$ stellar mass and halo occupation functions, and evolving cosmic star formation rate density (Vogelsberger et al. 2014), and Torrey et al. (2015b) showed that this parametrization produces galaxy populations that evolve consistently with observations.

In this section, we focus on the $z = 0$ spiral galaxies in Illustris to study the spiral arm morphology in multiple wavebands and explore its connection with BH and DM. Snyder et al. (2015) defined a non-parametric bulge strength parameter, $F(G, M_{20})$, to serve as a rough automated assessment of morphological types for the $z = 0$ galaxies in Illustris. In this parameter, G is the relative distribution of the galaxy pixel flux values (the Gini coefficient) and M_{20} is the second-order moment of the brightest 20 per cent of the galaxy's flux (Conselice et al. 2003; Lotz, Primack & Madau 2004). They found that late-type galaxies reside in the ($M_{20} < -2$, $G < 0.6$) region at $10.0 < \log(M_{\star,\,2R}/{\rm M}_\odot) < 11.0$. Following their definition for late-type galaxies, we first select 5131 galaxies from their *g*-band morphology catalogue, based on their location in the G–M_{20} plane. This sample includes a large number of galaxies with a 'ring-like' morphology or an irregular/disturbed shape (Vogelsberger et al. 2014; Snyder et al. 2015). About 10 per cent of disc galaxies in the mass range $M_{\star,\,2R} \sim 10^{10.5-11}\,{\rm M}_\odot$ exhibit strong stellar and gaseous ring-like features that are likely not realistic (Snyder et al. 2015). Hence, we use the face-on synthetic images in the Johnson *B* (444.9 nm) filter to construct a subsample of 2258 blue galaxies that do not have rings but display convincing evidence of definable spiral structure from image inspection. The methods of measuring spiral arm pitch angle are currently very much dependent on the visual inspection conducted by the user (Davis et al. 2012) and that makes a challenge to measure pitch angles for a large sample of the simulated galaxies. Therefore, we randomly select 95 galaxies out of our subsample and only attempt pitch angle measurements on these randomly selected galaxies. After constructing our spiral sample, we study the spiral arm morphology by using the face-on synthetic images in the Johnson *B* (444.9 nm), Cousins *R* (659.9 nm), and Johnson *K* (2.2 μm) filters, which are available at the Illustris web page (http://www.illustris-project.org/galaxy_obs/; Torrey et al. 2015a). For brevity, we only use the data reported for the face-on viewing direction, i.e. camera index = 3, since our algorithm requires image deprojection as this produces the most accurate results (Davis et al. 2012). Fig. 1 shows example images in the *B*, *R*, and *K* filters (from left to right) of the $z = 0$ Illustris galaxies, arranged by increasing stellar mass from top ($M_{\star,\,2R} \sim 10^{10}\,{\rm M}_\odot$) to bottom ($M_{\star,\,2R} \sim 10^{11}\,{\rm M}_\odot$). The remainder of this section analyses

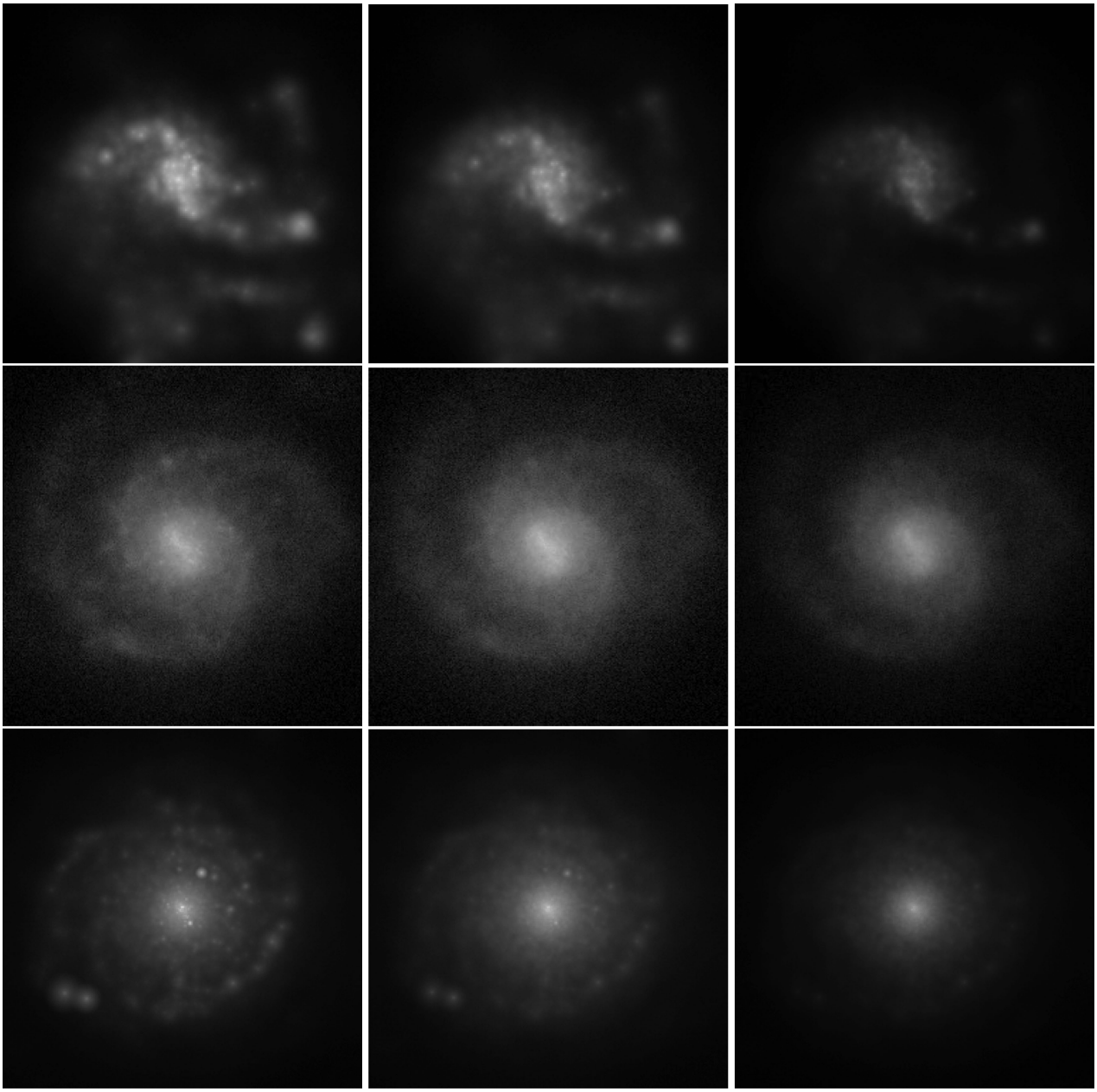

Figure 1. Example images in the *B*, *R*, and *K* filters of the $z = 0$ Illustris galaxies are shown from left to right, respectively. Top: ID = 450471; middle: ID = 41098; bottom: ID = 339972. They are arranged by increasing stellar mass from top ($M_{\star,\,2R} \sim 10^{10}\,\mathrm{M}_{\odot}$) to bottom ($M_{\star,\,2R} \sim 10^{11}\,\mathrm{M}_{\odot}$). Note that each image has a size of 256 pixels.

measurements of synthetic images that are most like those in this figure.

For our measurements, we employ the two-dimensional (2D) fast Fourier transform (FFT) software called P2DFFT.[1] This software is an updated version of 2DFFT (Davis et al. 2012) that implements parallel processing, allowing it to run faster than the serial 2DFFT, and has simplified the user input. See Saraiva Schroeder et al. (1994), Puerari & Dottori (1992), and Puerari et al. (2000) for more details on the 2DFFT algorithm. P2DFFT has been written to allow direct input of FITS images and optionally output inverse Fourier transform FITS images. Also included in the package is the ability to generate idealized logarithmic spiral test images of a specified size that have 1–6 arms with pitch angles of -75°–75°. P2DFFT further includes a PYTHON code that outputs Fourier amplitude versus inner radius and pitch angle versus inner radius for each Fourier component ($0 \leq m \leq 6$). This PYTHON routine also calculates the Fourier amplitude weighted mean pitch angle across $1 \leq m \leq 6$ versus inner radius.

Operationally, P2DFFT decomposes galaxy images into logarithmic spirals and determines the pitch angle that maximizes the Fourier amplitudes for each harmonic mode (m). This code provides a systematic way of excluding barred nuclei from the pitch angle measurement annulus by allowing inner radius to vary, and outputs the pitch angle as a function of inner radius. By using the face-on synthetic images, we avoid the deprojection process and any assumption related with it. Then, we seek a harmonic mode

[1] P2DFFT is available for download at https://treuthardt.github.io/P2DFFT/.

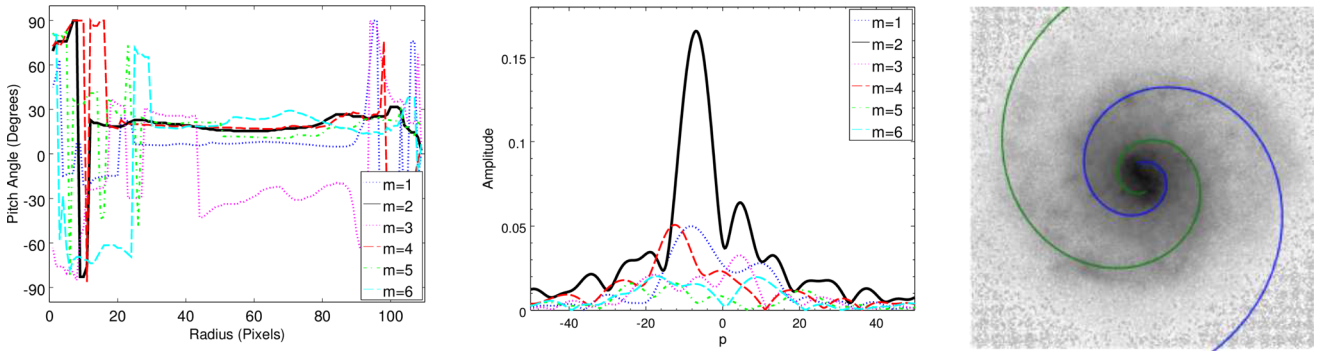

Figure 2. Left: example *B*-band pitch angle profile of a simulated spiral galaxy (ID = 41098) from our sample is shown as a function of inner radius. A stable mean pitch angle is determined for the $m = 2$ harmonic mode (solid black line): $P = 15.^{\circ}61 \pm 3.^{\circ}06$. Middle: the amplitude of each Fourier component for the *B*-band image of this simulated galaxy with a measurement annulus defined by an inner radius of 50 pixels and outer radius of 110 pixels. Right: an overlay image of a $15.^{\circ}61$ pitch angle spiral is shown on top of this simulated galaxy. Note that the image size is 256 pixels.

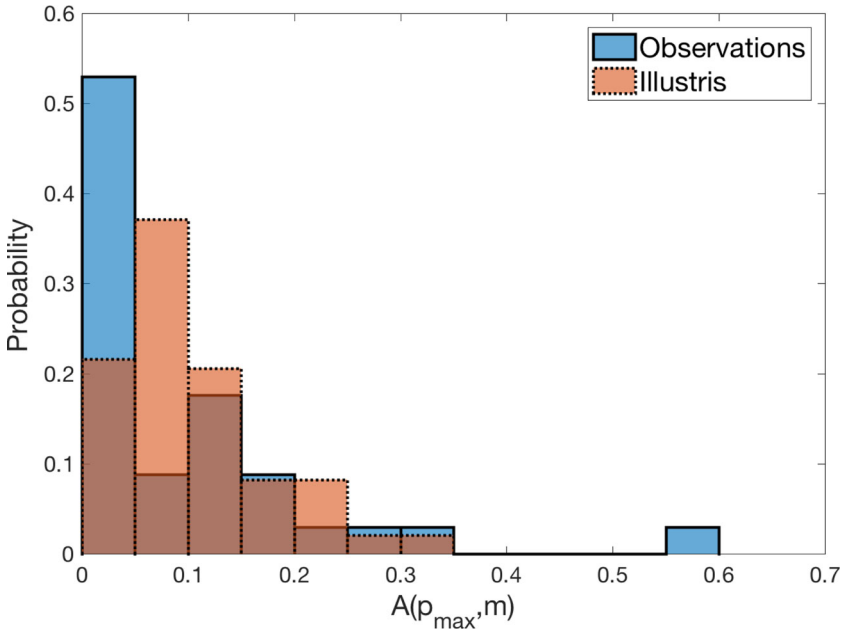

Figure 3. Comparison of the histograms of the $A(p_{\max}, m)$ values of our Illustris sample and the observed sample from Berrier et al. (2013) is shown. Our K–S test rejects the null hypothesis at the 5 per cent significance level. This agreement suggests that our comparison is meaningful.

in which pitch angle stays approximately constant over the largest range of radii, and measure pitch angle by averaging over this stable region. The error is determined by considering the size of the stable radius segment relative to the galaxy radius and the degree to which the stable segment is logarithmic (see Davis et al. 2012, for more detail). An example of our pitch angle measurements is shown in Fig. 2: a stable mean pitch angle is determined for the $m = 2$ harmonic mode from a minimum inner radius of 50 pixels to a maximum inner radius of 80 pixels, with an outer radius of 110 pixels. Note that the typical image size is 256 pixels. The middle panel shows the amplitude of each Fourier component with a measurement annulus defined by an inner radius of 50 pixels and an outer radius of 110 pixels. This clearly displays the dominance of the two-armed spiral harmonic mode. The same procedure is used for all 95 galaxies in the *B*, *R*, and *K* filters. Fig. 3 shows the comparison between the histograms of the $A(p_{\max}, m)$ values, i.e. the highest amplitude of the chosen harmonic mode (see Davis et al. 2012), for our Illustris sample and the observations reported by Berrier et al. (2013). We perform a Kolmogorov–Smirnov test (K–S test) by using MATLAB KSTEST2 task, which rejects the null hypothesis at the 5 per cent significance level. This agreement suggests that our comparison is meaningful. We also visually classify each galaxy as barred/non-barred according to the presence/absence of a clear sign of a bar structure. Our classification is based on visual inspection of the *K*-band images since near-infrared(NIR) bands show bars more frequently (Eskridge et al. 2000). We find a majority of our sample consisting of non-barred morphologies: 21 barred and 74 non-barred. This is in good agreement with the percentage of barred galaxies (29.4 ± 0.5) reported by Masters et al. (2011). The pitch angle measurements along with the data related with this paper are presented in Table 1.

It is important to investigate the possibility of different pitch angles arising in different wavebands of light. While optical *B*-band images tend to trace the bright massive star-forming regions of a galaxy, NIR images tend to trace the old stellar populations (and thus the spiral density wave) in galaxies (Seigar & James 1998; Eskridge et al. 2002). Moreover, a flocculent spiral structure in the *B*-band may appear as a grand design in the NIR imaging

Table 1. Our spiral galaxy sample. Columns: (1) Illustris subhalo ID. (2) Bar morphology: y for barred, n for non-barred. (3) Harmonic mode. (4) Highest amplitude of the chosen harmonic mode in the *B* band. (5) *B*-band pitch angle in degrees. (6) *R*-band pitch angle in degrees. (7) *K*-band pitch angle in degrees. (8) $M_{\rm BH}$ is the BH mass contained within the stellar half-mass radius, retrieved from the Illustris data base. (9)$M_{*,\,\rm total}$ is the total stellar mass bound to the subhalo, retrieved from the Illustris data base. (10) $M_{\rm DM}$ is the mass of dark matter bound to the subhalo, retrieved from the Illustris data base. (11) $M^{(2)}_{\rm halo}$, which is used in Section 2, is the total mass of all particles (all types) bound to the subhalo, retrieved from the Illustris data base. (12) $M^{(3)}_{\rm halo}$, which is used for central galaxies in Section 3, is the mass enclosed within a sphere, centred on the potential minimum of the halo, that has a mean internal density of 200 times the critical density of the Universe.

ID	Bar	m	$A(p_{\rm max}, m)$	P_B	P_R	P_K	$\log\left(\frac{M_{\rm BH}}{\rm M_\odot}\right)$	$\log\left(\frac{M_{*,\rm total}}{\rm M_\odot}\right)$	$\log\left(\frac{M_{\rm DM}}{\rm M_\odot}\right)$	$\log\left(\frac{M^{(2)}_{\rm halo}}{\rm M_\odot}\right)$	$\log\left(\frac{M^{(3)}_{\rm halo}}{\rm M_\odot}\right)$
(1)	(2)	(3)	(4)	(5)	(6)	(7)	(8)	(9)	(10)	(11)	(12)
41098	y	2	0.17	15.61 ± 3.06	14.65 ± 4.59	14.14 ± 4.21	8.08	11.07	11.89	11.96	–
66096	y	2	0.23	24.72 ± 3.44	22.44 ± 3.53	27.84 ± 3.82	6.49	10.18	11.46	11.55	–
167869	n	3	0.05	12.68 ± 1.12	9.60 ± 1.79	16.24 ± 1.88	7.61	10.82	11.68	11.75	–
183689	n	6	0.04	22.70 ± 1.65	22.34 ± 2.19	22.58 ± 2.30	7.31	10.77	11.62	11.69	–
250637	n	3	0.04	19.82 ± 3.64	21.67 ± 1.74	23.43 ± 2.43	7.22	10.82	11.64	11.72	–
274690	y	6	0.08	21.53 ± 3.89	22.32 ± 3.04	20.74 ± 1.69	7.04	10.30	11.67	11.72	–
278699	n	2	0.08	21.37 ± 3.65	22.72 ± 2.75	24.72 ± 2.13	7.83	11.10	11.72	11.83	–
287939	n	2	0.12	26.53 ± 3.43	26.06 ± 4.42	30.29 ± 2.83	7.14	10.18	11.31	11.37	–
292278	n	2	0.20	13.74 ± 3.78	13.24 ± 3.17	10.39 ± 2.20	8.06	10.97	12.14	12.18	–
293192	n	3	0.07	9.25 ± 2.82	9.22 ± 1.81	9.49 ± 3.17	7.84	11.06	12.23	12.27	–
295983	n	3	0.04	28.15 ± 3.38	27.00 ± 2.38	23.79 ± 3.98	7.12	10.24	11.25	11.34	–
308471	n	5	0.05	20.18 ± 1.00	19.96 ± 1.26	19.71 ± 2.64	7.76	10.69	12.11	12.14	–
315319	y	2	0.20	15.87 ± 1.24	16.18 ± 1.11	20.62 ± 3.06	7.46	10.96	11.95	12.03	–
318403	n	3	0.07	18.89 ± 3.65	16.76 ± 4.38	20.54 ± 3.04	7.64	11.01	12.21	12.25	–
339972	n	3	0.03	14.94 ± 1.39	14.41 ± 1.47	12.55 ± 3.27	8.28	11.12	12.61	12.63	12.56
348613	n	3	0.04	11.56 ± 2.99	10.51 ± 3.22	14.30 ± 1.73	8.24	10.97	12.58	12.60	12.55
349838	n	3	0.03	10.86 ± 1.88	10.76 ± 0.77	10.88 ± 0.60	8.07	10.89	12.58	12.60	12.53
353567	n	2	0.24	16.52 ± 1.92	16.67 ± 2.25	16.05 ± 2.82	7.69	11.09	12.43	12.46	12.39
357033	n	3	0.09	18.40 ± 1.88	19.08 ± 1.35	18.35 ± 4.08	7.94	10.86	12.36	12.38	12.35
360070	n	5	0.07	24.01 ± 1.45	24.32 ± 2.82	21.53 ± 3.60	7.73	11.02	12.43	12.46	12.38
365003	n	6	0.04	19.67 ± 1.60	20.43 ± 1.46	20.31 ± 1.63	7.53	10.78	12.34	12.38	12.39
373991	n	3	0.08	13.92 ± 3.32	17.14 ± 3.31	15.96 ± 3.04	8.26	10.98	12.43	12.44	12.39
376968	n	3	0.04	9.58 ± 1.89	9.42 ± 1.69	8.75 ± 2.47	8.05	11.09	12.36	12.39	12.36
377089	y	3	0.12	19.07 ± 3.58	21.96 ± 2.26	25.88 ± 2.24	7.51	10.86	12.20	12.24	12.29
379786	y	6	0.14	15.92 ± 2.21	18.31 ± 1.45	17.80 ± 1.11	7.79	10.94	12.34	12.37	12.31
381137	n	4	0.05	19.15 ± 2.90	18.24 ± 2.67	16.71 ± 2.76	7.93	10.88	12.37	12.39	12.35
390346	n	4	0.08	19.07 ± 2.32	18.62 ± 2.74	19.15 ± 2.40	7.74	10.79	12.19	12.23	12.18
393605	n	4	0.06	21.11 ± 1.41	22.38 ± 1.74	20.22 ± 2.60	7.50	10.82	12.15	12.18	12.14
393984	n	2	0.10	11.95 ± 1.23	11.35 ± 1.82	10.95 ± 2.39	7.84	10.90	12.24	12.27	12.21
396937	n	3	0.04	14.52 ± 2.82	15.31 ± 2.89	13.50 ± 3.55	8.15	10.80	12.28	12.30	12.24
397204	n	3	0.05	19.09 ± 3.11	18.50 ± 2.10	18.57 ± 1.17	7.60	10.70	12.21	12.24	12.21
397695	n	2	0.08	19.44 ± 2.16	21.75 ± 2.57	9.41 ± 3.38	7.79	10.77	12.14	12.17	12.13
400083	n	2	0.13	26.10 ± 3.28	27.10 ± 2.79	28.71 ± 1.28	6.94	10.56	11.99	12.05	12.14
401370	n	2	0.08	20.52 ± 1.47	21.07 ± 1.68	19.14 ± 1.78	7.61	10.82	12.18	12.21	12.16
401474	y	4	0.05	15.78 ± 2.38	17.23 ± 2.70	16.98 ± 1.52	7.78	10.94	12.19	12.21	12.17
401856	n	2	0.10	26.53 ± 3.43	26.06 ± 4.42	30.29 ± 2.83	6.51	10.16	11.88	11.91	12.21
403323	n	3	0.12	14.09 ± 1.46	13.98 ± 1.67	13.43 ± 1.33	7.88	10.91	12.17	12.21	12.16
403642	n	2	0.11	20.34 ± 3.03	19.82 ± 4.07	15.83 ± 4.13	7.62	10.79	12.15	12.18	12.12
406286	n	3	0.06	20.68 ± 1.72	20.73 ± 2.51	20.02 ± 2.77	7.69	10.91	12.17	12.20	12.15
407890	n	3	0.21	16.89 ± 2.51	19.20 ± 2.62	24.23 ± 2.76	7.55	10.77	12.14	12.18	12.14
408954	n	3	0.10	20.02 ± 3.13	18.23 ± 3.59	18.86 ± 3.45	7.18	10.75	11.85	11.91	11.94
412343	n	2	0.19	23.86 ± 3.66	21.81 ± 2.31	15.16 ± 2.14	7.19	10.71	12.00	12.06	11.99
412515	n	4	0.09	27.73 ± 3.68	28.19 ± 3.88	23.35 ± 3.18	7.28	10.84	12.02	12.08	12.04
416531	y	4	0.16	24.36 ± 2.73	22.53 ± 1.43	21.04 ± 1.47	7.63	10.86	12.05	12.09	12.09
417495	n	3	0.07	15.75 ± 3.14	17.46 ± 2.28	20.01 ± 3.04	7.56	10.77	12.04	12.07	12.02
417736	n	4	0.05	20.52 ± 1.36	20.96 ± 2.05	17.83 ± 2.83	7.39	10.91	12.00	12.05	12.01
420546	n	4	0.09	18.29 ± 3.48	17.77 ± 3.49	19.11 ± 3.58	7.64	10.64	12.05	12.08	12.04
429333	n	4	0.03	16.55 ± 3.21	16.42 ± 2.11	20.93 ± 2.49	7.57	10.77	12.00	12.03	11.98
432924	n	4	0.09	20.51 ± 2.85	11.44 ± 1.81	25.16 ± 3.48	7.50	10.54	12.00	12.03	12.01
437478	y	2	0.27	23.92 ± 3.33	24.59 ± 3.15	26.14 ± 2.60	7.02	10.33	11.92	11.97	11.93
437661	n	3	0.03	25.66 ± 2.72	25.34 ± 2.39	29.96 ± 2.99	6.39	10.20	11.78	11.83	11.87
445191	n	5	0.03	34.62 ± 2.89	34.82 ± 3.15	30.00 ± 3.95	6.90	10.24	11.83	11.87	11.86
450471	y	3	0.22	19.62 ± 3.12	13.49 ± 1.19	12.33 ± 1.31	6.67	10.34	11.69	11.76	11.76
450907	y	5	0.08	26.75 ± 1.91	24.89 ± 3.32	27.30 ± 2.91	7.15	10.23	11.86	11.89	11.83
453583	n	4	0.07	18.43 ± 1.51	18.31 ± 1.75	21.23 ± 2.86	6.90	10.11	11.59	11.63	11.56
458148	n	2	0.14	16.86 ± 2.23	18.38 ± 2.79	23.43 ± 2.83	7.20	10.24	11.83	11.87	11.84

Table 1 – *continued*

ID	Bar	m	$A(p_{\max}, m)$	P_B	P_R	P_K	$\log\left(\frac{M_{\rm BH}}{\rm M_\odot}\right)$	$\log\left(\frac{M_{*,\rm total}}{\rm M_\odot}\right)$	$\log\left(\frac{M_{\rm DM}}{\rm M_\odot}\right)$	$\log\left(\frac{M^{(2)}_{\rm halo}}{\rm M_\odot}\right)$	$\log\left(\frac{M^{(3)}_{\rm halo}}{\rm M_\odot}\right)$
(1)	(2)	(3)	(4)	(5)	(6)	(7)	(8)	(9)	(10)	(11)	(12)
461309	n	3	0.06	20.93 ± 2.86	22.48 ± 2.71	18.47 ± 2.50	7.48	10.26	11.85	11.87	11.79
461677	y	2	0.16	16.62 ± 3.31	14.96 ± 2.63	21.96 ± 2.68	7.01	10.28	11.75	11.80	11.79
466545	n	2	0.12	10.37 ± 3.19	13.03 ± 2.08	13.75 ± 3.74	7.43	10.28	11.81	11.84	11.79
468379	n	3	0.18	23.72 ± 2.86	25.19 ± 2.52	26.15 ± 2.71	7.03	10.20	11.77	11.80	11.77
468683	n	4	0.21	24.03 ± 2.38	23.42 ± 1.07	28.52 ± 2.65	6.53	10.14	11.64	11.70	11.65
470338	n	5	0.09	25.04 ± 2.56	27.04 ± 2.84	21.17 ± 2.40	6.49	10.19	11.55	11.61	11.57
474123	y	5	0.09	18.92 ± 2.72	16.27 ± 3.99	14.73 ± 1.75	6.82	10.08	11.69	11.74	11.69
474359	y	2	0.30	23.49 ± 3.71	17.74 ± 1.67	15.34 ± 2.59	6.92	10.28	11.70	11.74	11.70
474410	y	3	0.07	15.89 ± 1.17	18.64 ± 1.35	21.59 ± 2.66	7.02	10.16	11.75	11.78	11.73
475081	n	2	0.33	16.12 ± 2.27	14.13 ± 3.12	12.95 ± 3.37	7.06	10.18	11.69	11.73	11.65
475122	y	6	0.06	38.00 ± 1.95	29.95 ± 3.39	35.60 ± 3.88	6.51	10.21	11.56	11.62	11.58
475149	n	4	0.10	15.39 ± 2.94	13.19 ± 2.91	21.40 ± 5.24	7.11	10.12	11.72	11.75	11.72
478250	n	5	0.03	29.62 ± 3.02	29.58 ± 2.33	28.16 ± 3.41	6.98	10.24	11.58	11.64	11.61
478741	n	4	0.18	24.89 ± 2.65	24.03 ± 3.30	26.45 ± 3.33	6.85	10.20	11.62	11.68	11.65
479639	n	4	0.03	28.21 ± 3.35	24.17 ± 1.93	23.89 ± 1.88	7.27	10.14	11.67	11.71	11.67
480862	n	5	0.14	19.05 ± 2.45	18.53 ± 2.39	18.42 ± 1.74	6.90	10.09	11.59	11.65	11.66
484500	n	2	0.14	20.03 ± 2.20	22.26 ± 2.44	19.66 ± 2.40	7.07	10.23	11.64	11.68	11.62
484893	n	2	0.10	19.36 ± 2.88	18.85 ± 3.26	22.50 ± 2.71	6.88	10.13	11.60	11.64	11.63
487035	y	5	0.03	29.60 ± 3.77	30.11 ± 2.19	22.63 ± 2.63	6.84	10.09	11.50	11.56	11.50
487887	n	5	0.16	30.34 ± 3.82	27.40 ± 3.71	28.92 ± 3.80	6.22	10.11	11.50	11.58	11.54
488002	y	4	0.13	29.43 ± 3.18	29.33 ± 2.54	29.41 ± 2.72	6.10	10.14	11.50	11.58	11.55
488826	y	2	0.09	17.42 ± 1.53	17.56 ± 1.92	15.35 ± 2.46	6.87	10.12	11.62	11.66	11.62
489973	n	6	0.06	29.76 ± 3.38	28.53 ± 3.26	29.50 ± 3.92	6.80	10.15	11.48	11.54	11.53
491764	n	3	0.04	23.95 ± 2.85	23.22 ± 2.06	24.11 ± 2.93	6.10	10.05	11.48	11.56	11.52
492528	n	2	0.09	20.13 ± 2.72	21.20 ± 2.97	30.20 ± 3.95	6.26	10.53	11.36	11.44	11.47
493024	n	3	0.22	26.17 ± 2.65	23.69 ± 2.11	19.35 ± 2.75	7.06	10.15	11.61	11.64	11.58
493332	n	3	0.10	18.64 ± 1.36	17.55 ± 1.81	18.47 ± 2.57	7.06	10.13	11.63	11.66	11.63
494358	n	3	0.07	13.96 ± 2.19	13.58 ± 1.35	19.72 ± 3.32	7.21	10.11	11.61	11.64	11.59
494540	n	3	0.10	17.63 ± 1.77	22.04 ± 2.29	24.33 ± 2.25	6.63	10.08	11.55	11.60	11.56
494646	n	2	0.16	26.69 ± 2.80	27.08 ± 2.54	24.65 ± 2.97	6.71	10.15	11.52	11.58	11.54
497326	y	3	0.10	20.29 ± 3.60	22.02 ± 2.47	23.59 ± 2.39	6.66	10.14	11.46	11.53	11.51
498275	n	4	0.03	23.98 ± 2.60	24.93 ± 2.54	24.20 ± 2.76	6.95	10.12	11.53	11.56	11.53
501185	n	4	0.05	20.07 ± 2.69	24.06 ± 1.80	26.24 ± 1.84	6.65	10.12	11.47	11.53	11.53
503382	y	3	0.10	28.60 ± 4.40	26.64 ± 3.20	33.69 ± 2.89	6.13	10.16	11.37	11.46	11.44
506252	n	6	0.07	25.98 ± 3.01	29.48 ± 3.11	31.74 ± 3.22	6.22	10.08	11.45	11.51	11.47
508079	n	5	0.03	28.40 ± 1.99	29.06 ± 2.14	32.23 ± 2.66	6.60	10.16	11.39	11.46	11.46
510148	n	3	0.07	29.32 ± 2.91	28.30 ± 2.50	27.73 ± 2.51	6.97	10.17	11.36	11.44	11.43
518358	n	4	0.02	23.58 ± 2.65	25.04 ± 2.29	26.94 ± 2.85	6.71	10.14	11.33	11.40	11.39
522537	n	4	0.03	31.95 ± 2.68	29.21 ± 4.36	28.26 ± 2.45	6.36	10.14	11.26	11.34	11.34

(Thornley 1996). Seigar et al. (2006) demonstrated the existence of a 1:1 relation between the *B*- and NIR band (either $K_{\rm s}$ or *H*) pitch angles for a sample of 66 galaxies from a combination of the Carnegie–Irvine Galaxy Survey (Ho et al. 2011) and the Ohio State University Bright Spiral Galaxy Survey (Eskridge et al. 2002). Later, Davis et al. (2012) confirmed this relation (between *B* and *I*) by remeasuring a subset of 47 galaxies of the galaxies appearing in Seigar et al. (2006). Note that Seigar et al. (2006) used an earlier version of the 2DFFT method and Davis et al. (2012) used a method similar to ours. Recently, Pour-Imani et al. (2016) found a modest difference between the bands at the extreme ends of this range, from *B* to 3.6 μm, but concluded that their results are consistent with the results of Seigar et al. (2006) and Davis et al. (2012) because of the small difference they recovered. Here we carefully investigate the simulated spiral arms when viewed in different wavebands and check if Illustris establishes a 1:1 relation that is expected from the observations. Fig. 4 presents our pitch angle measurements in different wavebands, showing that pitch angles are similar whether measured in the optical or NIR regimes. Although there are small-scale differences between spiral arms in different wavebands of the optical–NIR spectrum, the absence of a systematic behaviour in pitch angle values (such as being above or below relative to the 1:1 relation line) is consistent with the observational findings of Seigar et al. (2006) and Davis et al. (2012). The overall structure of the simulated spiral arms is consistent across the optical–NIR spectrum. Furthermore, neither barred (green stars) nor non-barred galaxies (black circles) show a significant difference in pitch angle in different wavebands. This implies that pitch angle derived is not biased by a presence of a bar. In addition, the most common *K*-band pitch angle in our sample is 21°, which is very close to the most probable pitch angle of 18.°52 that Davis et al. (2014) derived from a statistically complete collection of the brightest spiral galaxies.

2.2 Pitch angle scaling relations

Observational evidence shows a tight correlation between pitch angle and the central BH mass in disc galaxies (Seigar et al. 2006; Berrier et al. 2013). It has been shown empirically that there is a link

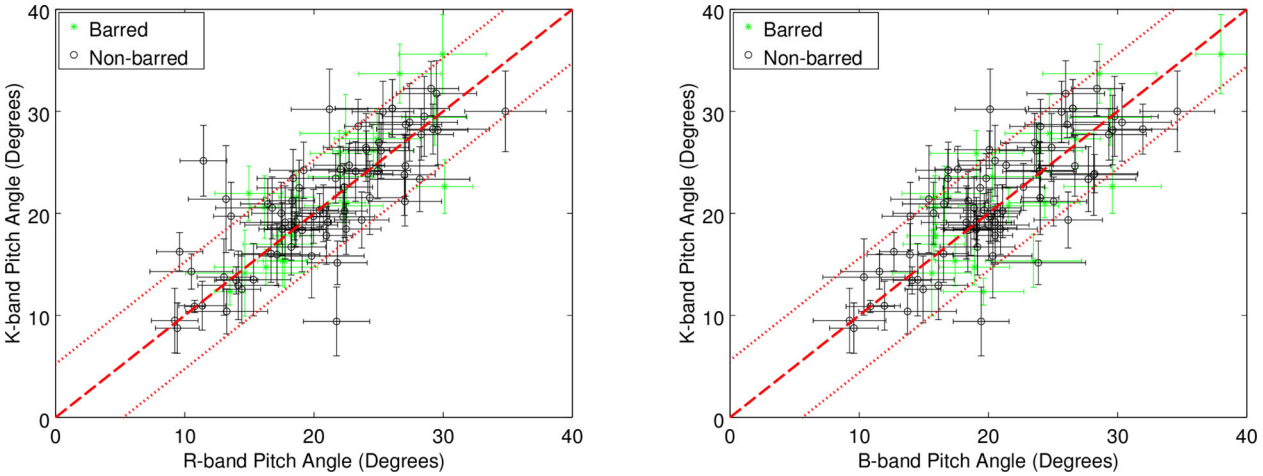

Figure 4. The pitch angle measurements for our spiral sample are shown in different wavebands (left: K versus R; right: K versus B). Galaxies with bars are shown by green stars. Galaxies with no clear sign of a bar are shown by black circles. The total rms scatter is plotted in dotted red lines above and below the 1:1 relation line (dashed red line): $5\overset{\circ}{.}24$ in K versus R and $5\overset{\circ}{.}60$ in K versus B. Although there are small-scale differences between spiral arms in different wavebands of the optical–NIR spectrum, the overall structure of the simulated spiral arms is consistent across the optical–NIR spectrum, which is consistent with the observational findings of Seigar et al. (2006) and Davis et al. (2012).

between pitch angle and the central mass concentration of galaxies (Seigar et al. 2005, 2006). Also, the supermassive BH–bulge connection is widely established as a result of observed correlations of the BH mass with $\sigma_{\rm sph}$, $M_{\rm sph}$, and $L_{\rm sph}$. Since both the BH mass and pitch angle are intimately related to the central mass concentration, it is no surprise that they correlate with each other quite strongly. For this relation, Berrier et al. (2013) reported a scatter less than 0.48 dex, which is lower than the intrinsic scatter ($\approx$0.56 dex) of the $M_{\rm BH}$–$\sigma_{\rm sph}$ relation, using only late-type galaxies (Gültekin et al. 2009). While pitch angle depends inversely on central bulge mass in bulge-dominated galaxies, it correlates to relative concentration of mass towards the galaxy's centre in disc-dominated galaxies, especially the extreme case of bulgeless galaxies (Berrier et al. 2013). Unfortunately, the relation between the BH mass and galaxy characteristics in disc-dominated galaxies is not clear empirically since relatively few BH masses have been directly measured in such galaxies.

We adopt $M_{\rm BH}$ directly from the simulation outputs as the BH mass contained within the stellar half-mass radius. For a given simulated galaxy, we define $M_{\rm DM}$ as the total mass of dark matter and $M_{\rm halo}$ as the total mass of all particles (all types) bound to the subhalo. We use the K-band pitch angle values in the scaling relations. In Fig. 5, we show the Illustris prediction (solid blue line) for the BH mass relative to pitch angle for our spiral sample, and compare it with the observed $M_{\rm BH}$–P relation (solid red line) by Berrier et al. (2013). The agreement between the Illustris result and the observations is very good: the slope and normalization of the observed $\log(M_{\rm BH}/{\rm M}_{\odot})$–$P$ relation are -0.062 ± 0.009 and 8.21 ± 0.16, respectively, whereas the simulation predicts -0.055 ± 0.001 and 8.40 ± 0.01. The Illustris best fit is obtained using the robust linear least-squares fitting method (i.e. bisquare weights) in MATLAB Curve Fitting Toolbox [goodness of fit: $R^2 = 0.36$, root-mean-square error (RMSE) = 0.44]. We use the same fitting method throughout this paper.

In Fig. 6, we display the Illustris predictions for DM mass and halo mass relative to pitch angle for our spiral sample. The simulation predicts a very tight correlation between these parameters: the slope and normalization are -0.029 ± 0.001 and 12.46 ± 0.01 ($R^2 = 0.22$, RMSE = 0.30) for the $\log(M_{\rm DM}/{\rm M}_{\odot})$–$P$ relation, respectively, whereas -0.027 ± 0.001 and 12.47 ± 0.01 ($R^2 = 0.21$, RMSE = 0.29) for the $\log(M_{\rm halo}/{\rm M}_{\odot})$–$P$ relation. It is especially interesting that Illustris predicts a tighter correlation between pitch angle and DM mass (and halo mass) when compared to the relation between pitch angle and the BH mass. This suggests that pitch angle can be used as a proxy for the DM mass (and halo mass) of disc galaxies. However, we emphasize that there is a large scatter in the DM mass (and halo mass) at fixed pitch angle.

Based on limited data, Seigar et al. (2014) uncovered a weak trend between pitch angle (used as a proxy for the BH mass) and DM concentration such that galaxies with tightly wound arms have particularly high concentrations. Furthermore, cosmological simulations often reveal an anticorrelation between DM mass and concentration (e.g. Bullock et al. 2001; van den Bosch et al. 2014). Here, we show that the Illustris simulation results in an anticorrelation between DM mass and pitch angle for our spiral sample (see Fig. 6). In conjunction with the DM mass versus concentration anticorrelation (Bullock et al. 2001; van den Bosch et al. 2014) and a DM mass versus pitch angle correlation (Fig. 6), we expect to derive a positive correlation between pitch angle and DM concentration. This is opposite to the weak trend presented in Seigar et al. (2014). However, given the large scatter in the DM mass versus concentration relations revealed by the simulations, and the limitations of the observational data discussed by Seigar et al. (2014) no strong conclusions can be made. Indeed, Seigar et al. (2014) commented that more observational data are needed to really test the predictions made in theoretical studies, such that it would be possible to truly determine, observationally, how DM mass and pitch angle are related or, indeed, if they are related. Moreover, it would be worth testing this link with the future Illustris DM halo catalogues (Chua et al. 2017) in a future study.

Many works (e.g. Graham 2008; Hu 2008; Gültekin et al. 2009; Graham & Scott 2013) have identified an offset in the supermassive BH–bulge relations between galaxies with barred and non-barred morphologies. For the pitch angle scaling relations, we find no offset between the barred (green stars) and non-barred (black circles) galaxies of our spiral sample in Illustris.

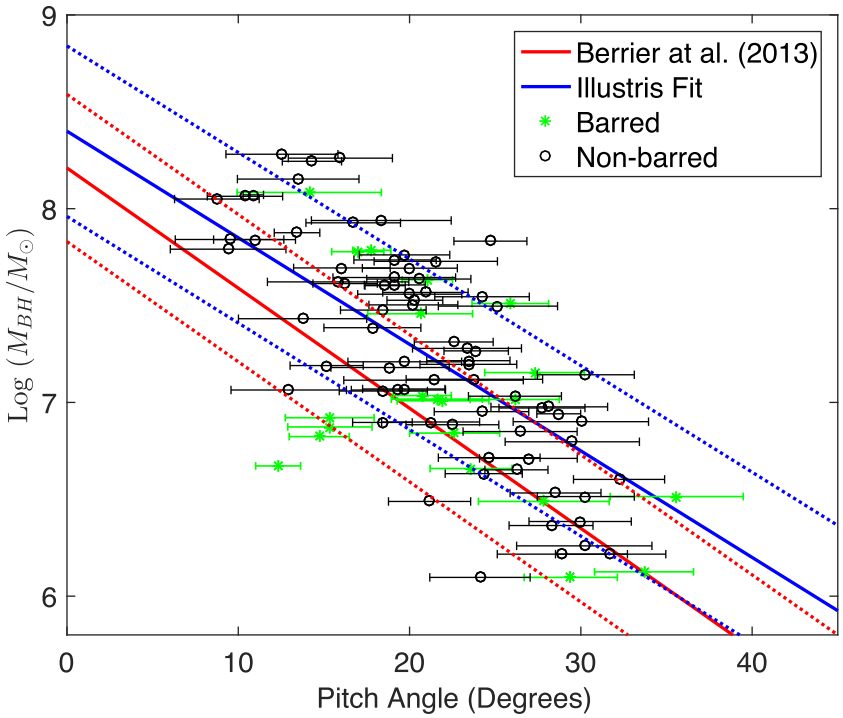

Figure 5. The Illustris prediction for the BH mass relative to pitch angle for our spiral sample is shown by the solid blue line, which represents the best fit to the data. Galaxies with bars are shown by green stars. Galaxies with no clear sign of a bar are shown by black circles. The total rms scatter of ±0.44 dex in the $\log(M_{\rm BH}/{\rm M}_\odot)$ direction is plotted in dotted blue lines above and below the best-fitting line. For comparison, we have also plotted the observed $M_{\rm BH}$–P relation by Berrier et al. (2013), represented by the solid red line and bounded by its ±0.38 dex rms scatter in the $\log(M_{\rm BH}/{\rm M}_\odot)$ direction, above and below with dotted red lines. Overall, the Illustris simulation reproduces the observed relation very well for disc galaxies.

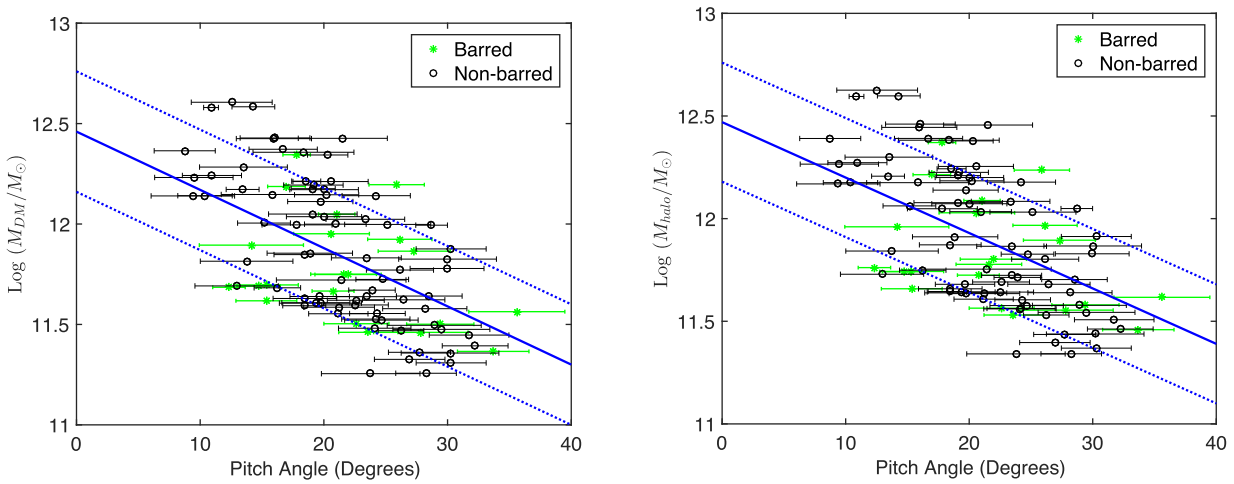

Figure 6. The Illustris predictions for the DM mass and halo mass relative to pitch angle for our spiral sample are shown by the solid blue lines, which represent the best fits to the data: left is the $M_{\rm DM}$–P relation and right is the $M_{\rm halo}$–P relation. Galaxies with bars are shown by green stars. Galaxies with no clear sign of a bar are shown by black circles. The total rms scatters are plotted as dotted blue lines above and below the best-fitting lines: ±0.30 dex in the $\log(M_{\rm DM}/{\rm M}_\odot)$ direction and ±0.29 dex in the $\log(M_{\rm halo}/{\rm M}_\odot)$ direction. Note that the Illustris predictions for these correlations are tighter than the one between pitch angle and the BH mass.

3 BLACK HOLE SCALING RELATIONS BEYOND THE BULGE

In this section, we focus on the $z = 0$ Illustris central galaxies with $10.0 < \log(M_{\star,\,2R}/{\rm M}_\odot) < 13.0$ to study the BH mass scaling relations beyond the bulge, i.e. the $M_{\rm BH}$–$M_{\star,\,\rm total}$, the $M_{\rm BH}$–$M_{\rm DM}$, and $M_{\rm BH}$–$M_{\rm halo}$ relations. We adopt $M_{\star,\,\rm total}$ directly from the simulation outputs as the total mass of the stellar particles bound to the subhalo. Here, we only investigate central galaxies, i.e. the main halo of each friend-of-friends (FoF) group, in order to avoid satellite galaxies for which the halo mass is poorly defined and much of the mass may be assigned to the parent halo. In our spiral sample, there are 81 central galaxies: 17 barred and 64 non-barred. In this section, we only display these central spiral galaxies. Note that Snyder et al. (2015) also presented these relations as a function of galaxy morphology. Here, we investigate these predictions by

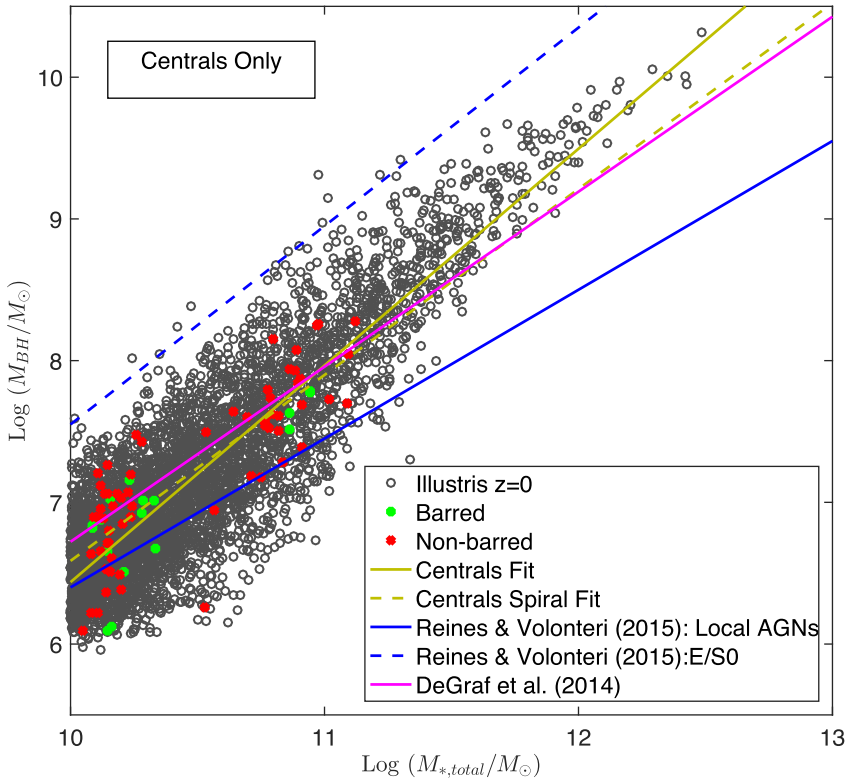

Figure 7. The Illustris prediction of the $M_{\rm BH}$–$M_{\star,\,\rm total}$ relation for central galaxies is shown by the solid yellow line, which represents the best fit to the simulated data: the slope and normalization are 1.53 ± 0.02 and -8.85 ± 0.26 ($R^2 = 0.75$, RMSE $= 0.36$) for the $\log(M_{\rm BH}/{\rm M}_{\odot})$–$\log(M_{\star,\,\rm total}/{\rm M}_{\odot})$ relation. While the red crosses indicate our non-barred spiral sample from Illustris, the green filled circles indicate barred ones. The best fit to our spiral sample is shown by the dashed yellow line. For comparison, we plot the observed $M_{\rm BH}$–$M_{\star,\,\rm total}$ relations by Reines & Volonteri (2015), represented by the solid blue line for local AGNs and the dashed blue line for E/S0 galaxies. These authors also suggested that spirals and discs follow the same relation with local AGNs. We also compare with the relation by DeGraf et al. (2015) from the high-resolution cosmological simulation MassiveBlackII, represented by the magenta line.

comparing them with other theoretical results and observational constraints at $z = 0$. The aim is to clearly understand these different relations, e.g. which one may be the strongest correlation, whether different galaxy types exhibit weaker/stronger physical links with their BHs. Moreover, a better understanding of the relations beyond the bulge could provide a benchmark for high-redshift studies that cannot avail themselves of bulge masses or dynamical BH masses (Reines & Volonteri 2015).

3.1 The $M_{\rm BH}$–$M_{\star,\rm total}$ relation

In Fig. 7, we display the Illustris prediction of the $M_{\rm BH}$–$M_{\star,\,\rm total}$ relation for central galaxies with the solid yellow line, which presents the best fit to the simulation data: $\log(M_{\rm BH}/{\rm M}_{\odot}) = (1.53 \pm 0.02)\log(M_{\star,\,\rm total}/{\rm M}_{\odot}) - (8.85 \pm 0.26)$, with $R^2 = 0.75$, RMSE $= 0.36$. For comparison, we have also plotted the observed $M_{\rm BH}$–$M_{\star,\,\rm total}$ relations by Reines & Volonteri (2015), which used a sample of 262 local broad-line AGN and 79 galaxies with dynamical BH masses. Their total stellar mass measurements rely on mass-to-light ratios. The authors defined a relation for AGN host galaxies (solid blue line) that has a similar slope to early-type galaxies with quiescent BHs (dashed blue line), but a normalization that is more than an order of magnitude lower. They also suggested that a potential origin for these different relations could be differences in host galaxy properties (e.g. the Hubble types), claiming that spirals/discs tend to overlap with AGN host galaxies. Although the Illustris galaxies lie within the observational relations of Reines & Volonteri (2015), it seems that Illustris underestimates the BH masses of early-type galaxies for a given $M_{\star,\,\rm total}$ when compared to the observational relation (dashed blue line). Moreover, Illustris appears to favour a single linear relation for all galaxy types, disagreeing with the findings of Reines & Volonteri (2015). To explore the relation based on bar morphology, the barred and non-barred spiral galaxies in our sample are depicted by different signs (green dots and red crosses, respectively). The dashed yellow line is the best fit to our spiral sample, which is consistent with the best fit that is obtained from all galaxy types. Note that the apparent scarcity of the galaxies with $M_{\star,\,\rm total} \sim 10^{10.5}\,{\rm M}_{\odot}$ in our spiral sample is due to the high abundance of the peculiar galaxies, i.e. ringed galaxies, in this mass range (Snyder et al. 2015). We also compare with the prediction of the high-resolution cosmological simulation MassiveBlackII (DeGraf et al. 2015), showing remarkable agreement with the Illustris prediction with a slightly shallow slope (see the magenta line). Their relation, which is derived for all galaxy types, is in remarkable agreement with our best fit for our spiral sample. This supports the idea that BHs in spiral galaxies correlate with $M_{*,\,\rm total}$ in a similar way to those in early-type galaxies do. DeGraf et al. (2015) showed that the low end of their $M_{\rm BH}$–$\sigma_{\rm sph}$ relation tends to lie above the observations, which is consistent with Sijacki et al. (2015), who found similar behaviour at the low end. However, the authors showed that their $M_{\rm BH}$–$M_{\star,\,\rm total}$ relation shows good agreement with the observations at the high end and at the low end of the relation. Based on the consistent predictions between Illustris and MassiveBlackII, this also implies good agreement between Illustris and the observations for both ends of the relation.

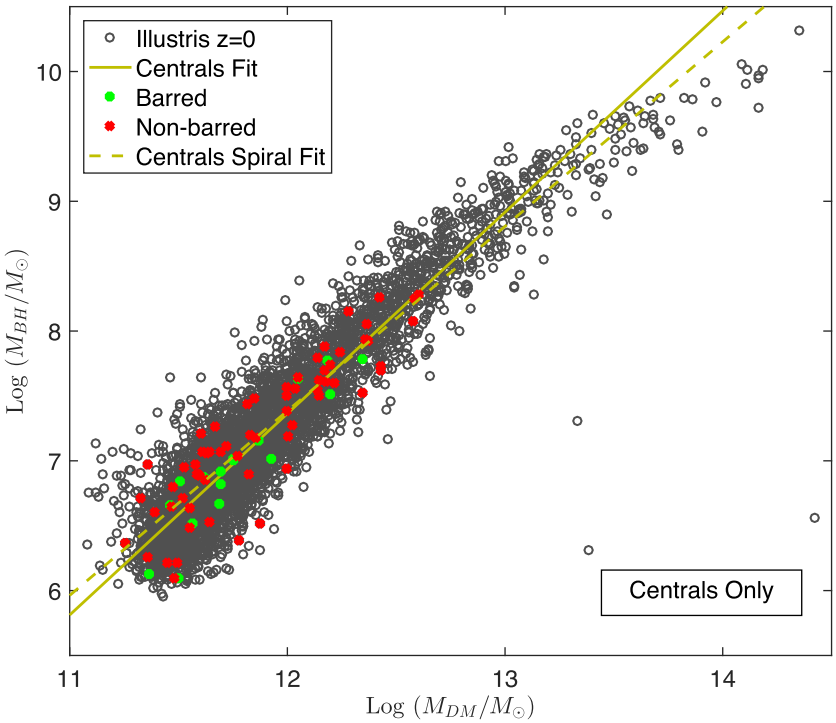

Figure 8. The Illustris prediction of the $M_{\rm BH}$–$M_{\rm DM}$ relation for central galaxies is shown by the solid yellow line, which represents the best fit to the simulated data: $\log(M_{\rm BH}/{\rm M}_\odot) = (1.55 \pm 0.02)\log(M_{\rm DM}/{\rm M}_\odot) - (11.26 \pm 0.20)$ ($R^2 = 0.88$, RMSE $= 0.25$). The dashed yellow line represents the best fit to our spiral sample, which is shown by the red crosses (non-barred) and the filled green circles (barred).

3.2 The $M_{\rm BH}$–$M_{\rm DM}$ relation

Fig. 8 shows the Illustris prediction of the $M_{\rm BH}$–$M_{\rm DM}$ relation for central galaxies. The best fit to the simulation data is $\log(M_{\rm BH}/{\rm M}_\odot) = (1.55 \pm 0.02)\log(M_{\rm DM}/{\rm M}_\odot) - (11.26 \pm 0.20)$, with $R^2 = 0.88$, RMSE $= 0.25$. The best fit to our simulated spiral sample is depicted by the dashed yellow line, which is very close to the one for all types (solid yellow line). Both the barred (green filled circles) and non-barred (red crosses) spirals follow the mean relation closely without falling systematically above or below the relation.

3.3 The $M_{\rm BH}$–$M_{\rm halo}$ relation

Here, we investigate the $M_{\rm BH}$–$M_{\rm halo}$ relation for central galaxies, where we adopt $M_{\rm halo}$ as the mass enclosed within a sphere, centred on the potential minimum of the halo, that has a mean internal density of 200 times the critical density of the Universe. Fig. 9 compares the Illustris prediction of the $M_{\rm BH}$–$M_{\rm halo}$ relation with other theoretical results and the observational constraints. Most self-regulating theoretical models of galactic physics predict a fundamental connection between the central BH mass and the total mass of the host galaxy (Haehnelt, Natarajan & Rees 1998; Silk & Rees 1998; Monaco, Salucci & Danese 2000; Adams, Graff & Richstone 2001; El-Zant et al. 2003). The galaxy models, which study the interaction between the DM haloes of galaxies and baryonic matter, predict that halo properties determine the masses of bulge and central BH (Cattaneo 2001; El-Zant et al. 2003; Hopkins et al. 2005). However, there are inconsistencies in the observational studies: while some studies argued for (Seigar 2011; Volonteri, Natarajan & Gültekin 2011), some argued against (Kormendy & Bender 2011) a coupling of the BH mass and the properties of the DM halo. It is not an easy task to investigate this relation observationally due to the uncertainties in measurement of the halo mass. Some of the first indirect observational evidence for the existence of a $M_{\rm BH}$–$M_{\rm halo}$ relation come from the study of Ferrarese (2002), which first derived a correlation between $\sigma_{\rm sph}$ and the galaxy's circular velocity ($v_{\rm c}$) for a sample of 20 elliptical galaxies and 16 spiral galaxies, then translated it to a $M_{\rm BH}$–$M_{\rm halo}$ relation. While using the $M_{\rm BH}$–$\sigma_{\rm sph}$ relation (Ferrarese & Merritt 2000) to estimate the BH mass, the author demonstrated the effect of the method used to connect $v_{\rm c}$ to $M_{\rm halo}$ via $v_{\rm vir}$. The solid magenta line shows the best-fitting $M_{\rm BH}$–$M_{\rm halo}$ relation obtained by Ferrarese (2002) using the cosmological prescription of Bullock et al. (2001) to relate $v_{\rm c}$ and $v_{\rm vir}$. The dashed magenta line shows the resulting relation if $v_{\rm vir}/v_{\rm c} = 1$ is assumed, while the dotted magenta line presents the resulting relation if $v_{\rm vir}/v_{\rm c} = 1.8$ is used, as proposed by Seljak (2002). Among the relations obtained by Ferrarese (2002), the Illustris prediction agrees better with the solid magenta line, i.e. the one derived from the cosmological prescription of Bullock et al. (2001). The solid cyan line is the best fit for Illustris central galaxies from Snyder et al. (2015), while the solid green line is our best fit: $\log(M_{\rm BH}/{\rm M}_\odot) = (1.62 \pm 0.02)\log(M_{\rm halo}/{\rm M}_\odot) - (12.07 \pm 0.23)$ ($R^2 = 0.85$, RMSE $= 0.28$). Note that Snyder et al. (2015) fitted the Illustris data by using orthogonal distance regression method (Boggs & Rogers 1990), while we used bisquare weights. Later, Bandara, Crampton & Simard (2009) investigated this relation by using gravitational lens modelling to determine the total mass. They estimated the BH masses from the $M_{\rm BH}$–$\sigma_{\rm sph}$ relation by Gültekin et al. (2009). They recovered a non-linear correlation between $M_{\rm BH}$ and $M_{\rm halo}$, suggesting a slope of $\sim$1.67 that implies a merger-driven, feedback regulated process for the growth of supermassive BHs. Based on their argument, the Snyder et al. (2015) fit with a slope of $\sim$1.69

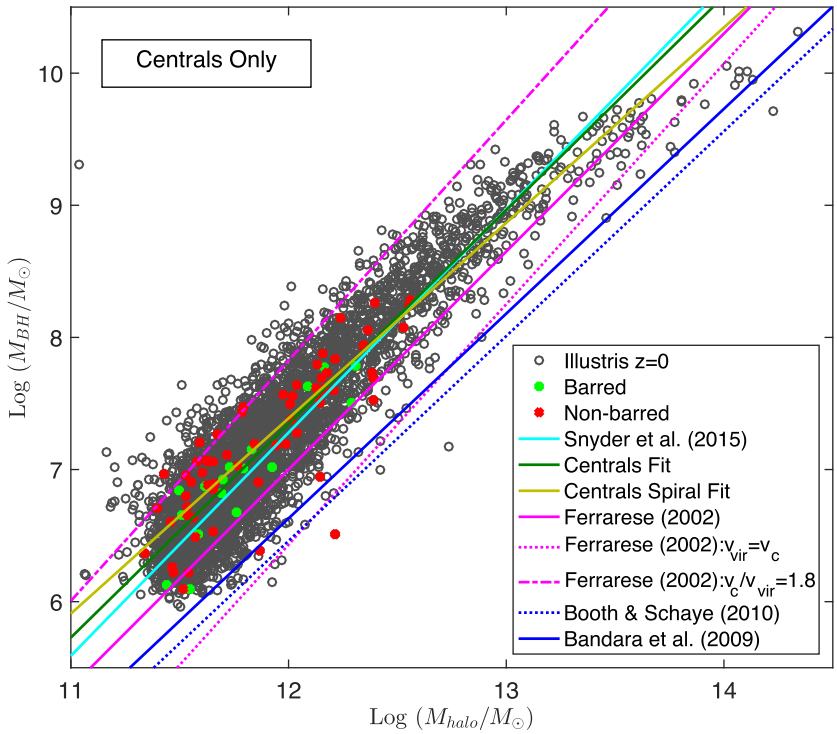

Figure 9. The Illustris prediction of the $M_{\rm BH}$–$M_{\rm halo}$ relation for central galaxies is compared with other theoretical predictions and the local observations. The solid cyan line is the best fit from Snyder et al. (2015), while the solid green line is our best fit for central galaxies. The solid yellow line is the best fit to our spiral sample, which is shown by the red crosses (non-barred) and green filled circles (barred). The magenta lines are same as in fig. 6 of Ferrarese (2002): the solid line corresponds to the best fit using the prescription of Bullock et al. (2001) to relate $v_{\rm vir}$ to $v_{\rm c}$, the dot–dashed line shows where the galaxies would lie if $v_{\rm vir} = v_{\rm c}$, and the dotted line shows where they would move to if $v_{\rm c}/v_{\rm vir} = 1.8$, as proposed by Seljak (2002). The solid blue line shows the observational determination of Bandara et al. (2009), while the dotted blue line shows the result from the simulation of Booth & Schaye (2010).

implies a merger-driven, feedback regulated process, and support the conclusion of Sijacki et al. (2015) that both BH feedback and BH–BH mergers are important ingredients to produce the $M_{\rm BH}$–$M_{\rm sph}$ relation. Using self-consistent simulations of the co-evolution of the BH and galaxy populations, Booth & Schaye (2010) demonstrated a very good agreement between the observational determination of Bandara et al. (2009) and their simulation when the simulation was only tuned to match the normalization of the relations between $M_{\rm BH}$ and the galaxy stellar properties. The mean Illustris trend seems to differ from those of Booth & Schaye (2010) and Bandara et al. (2009) by several standard deviations, but stays within the region defined by Ferrarese & Merritt (2000). In addition, Booth & Schaye (2010) suggested a primary link to halo binding energy rather than the halo mass, with the central halo concentration playing a role in the relation's scatter. It would be worth investigating this link with the future Illustris DM halo data catalogues (Chua et al. 2017) in a future study.

In addition, the best fit to our spiral sample, shown by the solid yellow line in Fig. 9, is consistent with the best fits to all galaxy types (solid cyan, green, and magenta lines), implying that spirals in Illustris follow the mean relation very closely. This suggests the existence of a tight correlation between the galactic properties of star-forming blue galaxies and their BHs. Also, we do not observe any systematic behaviour based on bar morphology such as being well above or below the mean relation, suggesting the presence or absence of a bar does not affect the link between the BH and its host galaxy significantly. Moreover, we highlight that the simulated galaxies present a smaller scatter around the mean $M_{\rm BH}$–$M_{\rm halo}$ relation when compared to the mean $M_{\rm BH}$–$M_{\star,\,\rm total}$ relation.

4 CONCLUSIONS

We investigate the supermassive BH–galaxy connection beyond the bulge in the high-resolution cosmological simulation Illustris. Our work is complementary to Sijacki et al. (2015), which studied the BH–bulge scaling relations as a function of galaxy morphology, colour, and specific star formation rate. Here we study these predictions by comparing with other theoretical results and observational constraints at $z = 0$.

First, we use a randomly selected sample of Illustris spiral galaxies that do not have rings, and study the spiral arm morphology in multiple wavebands. We present the existence of a 1:1 relation between the *B*- and *K*-band pitch angles of our sample in Illustris, which is consistent with the observational findings of Seigar et al. (2006) and Davis et al. (2012). Then, we explore the Illustris predictions for the BH mass, DM mass, and halo mass relative to pitch angle for our spiral sample. We derive an Illustris prediction of the $M_{\rm BH}$–P relation that is consistent with observational constraints. More importantly, we obtain a tighter correlation between pitch angle and DM/halo mass. Based on the Illustris predictions, we conclude that pitch angle can be used as a tracer for DM/halo mass.

In addition, we focus on the $z = 0$ Illustris central galaxies with $10.0 < \log(M_{\star,\,2R}/{\rm M}_{\odot}) < 13.0$ to study the $M_{\rm BH}$–$M_{\star,\,\rm total}$, the $M_{\rm BH}$–$M_{\rm DM}$, and $M_{\rm BH}$–$M_{\rm halo}$ relations by comparing with other theoretical studies and observational constraints. We find that Illustris establishes very tight correlations between the BH mass and large-scale properties of the host galaxy, not only for early-type galaxies but also low-mass, blue and star-forming galaxies, regardless of bar morphology. The tight relations shown in this work are strongly

suggestive that halo properties play an important role in determining those of the galaxy and its supermassive BH.

ACKNOWLEDGEMENTS

BM-P and MSS wish to thank the generous support of the University of Minnesota, Duluth and the Fund for Astrophysical Research. We also wish to thank the anonymous referee whose comments greatly improved the content of this paper. We also thank Benjamin L. Davis for providing us the pitch angle measurements of Berrier et al. (2013).

This research has made use of the Illustris data base. The Illustris project acknowledges support from many sources: support by the DFG Research Centre SFB-881 'The Milky Way System' through project A1, and by the European Research Council under ERC-StG EXAGAL-308037, support from the *HST* grants program, number HST-AR-12856.01-A, support for program #12856 by NASA through a grant from the Space Telescope Science Institute, which is operated by the Association of Universities for Research in Astronomy, Inc., under NASA contract NAS 5-26555, support from NASA grant NNX12AC67G and NSF grant AST-1312095, support from the Alexander von Humboldt Foundation, NSF grant AST-0907969, and support from XSEDE grant AST-130032, which is supported by National Science Foundation grant number OCI-1053575. The Illustris simulation was run on the CURIE supercomputer at CEA/France as part of PRACE project RA0844, and the SuperMUC computer at the Leibniz Computing Centre, Germany, as part of project pr85je. Further simulations were run on the Harvard Odyssey and CfA/ITC clusters, the Ranger and Stampede supercomputers at the Texas Advanced Computing Center through XSEDE, and the Kraken supercomputer at Oak Ridge National Laboratory through XSEDE.

REFERENCES

Adams F. C., Graff D. S., Richstone D. O., 2001, ApJ, 551, L31
Bandara K., Crampton D., Simard L., 2009, ApJ, 704, 1135
Barth A. J., 2004, in Ho L. C., ed., Coevolution of Black Holes and Galaxies. Cambridge Univ. Press, Cambridge, p. 21
Berrier J. C. et al., 2013, ApJ, 769, 132
Boggs P., Rogers J., 1990, Contemporary Math., 112, 183
Booth C. M., Schaye J., 2009, MNRAS, 398, 53
Booth C. M., Schaye J., 2010, MNRAS, 405, L1
Bower R. G., Benson A. J., Malbon R., Helly J. C., Frenk C. S., Baugh C. M., Cole S., Lacey C. G., 2006, MNRAS, 370, 645
Bullock J. S., Kolatt T. S., Sigad Y., Somerville R. S., Kravtsov A. V., Klypin A. A., Primack J. R., Dekel A., 2001, MNRAS, 321, 559
Cattaneo A., 2001, MNRAS, 324, 128
Chua K. T. E., Pillepich A., Rodriguez-Gomez V., Vogelsberger M., Bird S., Hernquist L., 2017, MNRAS, 472, 4343
Ciotti L., Ostriker J. P., Proga D., 2009, ApJ, 699, 89
Conselice C. J., Bershady M. A., Dickinson M., Papovich C., 2003, AJ, 126, 1183
Croton D. J. et al., 2006, MNRAS, 365, 11
Davis B. L., Berrier J. C., Shields D. W., Kennefick J., Kennefick D., Seigar M. S., Lacy C. H. S., Puerari I., 2012, ApJS, 199, 33
Davis B. L. et al., 2014, ApJ, 789, 124
DeGraf C., Di Matteo T., Treu T., Feng Y., Woo J.-H., Park D., 2015, MNRAS, 454, 913
Di Matteo P., Combes F., Chilingarian I., Melchior A.-L., Semelin B., 2008, Astron. Nachr., 329, 952
Dubois Y., Pichon C., Haehnelt M., Kimm T., Slyz A., Devriendt J., Pogosyan D., 2012, MNRAS, 423, 3616
El-Zant A. A., Shlosman I., Begelman M. C., Frank J., 2003, ApJ, 590, 641
Eskridge P. B. et al., 2000, AJ, 119, 536
Eskridge P. B. et al., 2002, ApJS, 143, 73
Fanidakis N., Baugh C. M., Benson A. J., Bower R. G., Cole S., Done C., Frenk C. S., 2011, MNRAS, 410, 53
Ferrarese L., 2002, ApJ, 578, 90
Ferrarese L., Merritt D., 2000, ApJ, 539, L9
Gebhardt K. et al., 2000, ApJ, 539, L13
Gebhardt K., Adams J., Richstone D., Lauer T. R., Faber S. M., Gültekin K., Murphy J., Tremaine S., 2011, ApJ, 729, 119
Genel S. et al., 2014, MNRAS, 445, 175
Graham A. W., 2007, MNRAS, 379, 711
Graham A. W., 2008, ApJ, 680, 143
Graham A. W., Driver S. P., 2007, ApJ, 655, 77
Graham A. W., Scott N., 2013, ApJ, 764, 151
Graham A. W., Erwin P., Caon N., Trujillo I., 2001, ApJ, 563, L11
Graham A. W., Erwin P., Caon N., Trujillo I., 2003, in Avila-Reese V., Firmani C., Frenk C. S., Allen C., eds, Rev. Mex. Astron. Astrofis. Conf. Ser. Vol. 17, Galaxy Evolution: Theory & Observations. p. 196. Available at: http://www.astroscu.unam.mx/rmaa/
Gültekin K. et al., 2009, ApJ, 698, 198
Haehnelt M. G., Natarajan P., Rees M. J., 1998, MNRAS, 300, 817
Häring N., Rix H.-W., 2004, ApJ, 604, L89
Hirschmann M., Dolag K., Saro A., Bachmann L., Borgani S., Burkert A., 2014, MNRAS, 442, 2304
Ho L. C., Li Z.-Y., Barth A. J., Seigar M. S., Peng C. Y., 2011, ApJS, 197, 21
Hopkins P. F., Hernquist L., Cox T. J., Di Matteo T., Martini P., Robertson B., Springel V., 2005, ApJ, 630, 705
Hu J., 2008, MNRAS, 386, 2242
Khandai N., Di Matteo T., Croft R., Wilkins S., Feng Y., Tucker E., DeGraf C., Liu M.-S., 2015, MNRAS, 450, 1349
Kormendy J., 2004, in Ho L. C., ed., Coevolution of Black Holes and Galaxies. Cambridge Univ. Press, Cambridge, p. 1
Kormendy J., Bender R., 2011, Nature, 469, 377
Kormendy J., Ho L. C., 2013, ARA&A, 51, 511
Kormendy J., Richstone D., 1995, ARA&A, 33, 581
Lotz J. M., Primack J., Madau P., 2004, AJ, 128, 163
McConnell N. J., Ma C.-P., 2013, ApJ, 764, 184
McGaugh S. S., 2012, AJ, 143, 40
Magorrian J. et al., 1998, AJ, 115, 2285
Masters K. L. et al., 2011, MNRAS, 411, 2026
Monaco P., Salucci P., Danese L., 2000, MNRAS, 311, 279
Pour-Imani H., Kennefick D., Kennefick J., Davis B. L., Shields D. W., Shameer Abdeen M., 2016, ApJ, 827, L2
Puerari I., Dottori H. A., 1992, A&AS, 93, 469
Puerari I., Block D. L., Elmegreen B. G., Frogel J. A., Eskridge P. B., 2000, A&A, 359, 932
Reines A. E., Volonteri M., 2015, ApJ, 813, 82
Saraiva Schroeder M. F., Pastoriza M. G., Kepler S. O., Puerari I., 1994, A&AS, 108, 41
Savorgnan G. A. D., 2016, ApJ, 821, 88
Savorgnan G., Graham A. W., Marconi A., Sani E., Hunt L. K., Vika M., Driver S. P., 2013, MNRAS, 434, 387
Schaye J. et al., 2015, MNRAS, 446, 521
Seigar M. S., 2011, ISRN Astron. Astrophys., 2011, 725697
Seigar M. S., James P. A., 1998, MNRAS, 299, 685
Seigar M. S., Block D. L., Puerari I., Chorney N. E., James P. A., 2005, MNRAS, 359, 1065
Seigar M. S., Bullock J. S., Barth A. J., Ho L. C., 2006, ApJ, 645, 1012
Seigar M. S., Kennefick D., Kennefick J., Lacy C. H. S., 2008, ApJ, 678, L93
Seigar M. S., Davis B. L., Berrier J., Kennefick D., 2014, ApJ, 795, 90
Seljak U., 2002, MNRAS, 334, 797
Sijacki D., Springel V., Di Matteo T., Hernquist L., 2007, MNRAS, 380, 877
Sijacki D., Vogelsberger M., Genel S., Springel V., Torrey P., Snyder G. F., Nelson D., Hernquist L., 2015, MNRAS, 452, 575
Silk J., Rees M. J., 1998, A&A, 331, L1

Snyder G. F. et al., 2015, MNRAS, 454, 1886
Springel V., Di Matteo T., Hernquist L., 2005, MNRAS, 361, 776
Thornley M. D., 1996, ApJ, 469, L45
Torrey P. et al., 2015a, MNRAS, 447, 2753
Torrey P. et al., 2015b, MNRAS, 454, 2770
Tremaine S. et al., 2002, ApJ, 574, 740
Tully R. B., Fisher J. R., 1977, A&A, 54, 661
van den Bosch F. C., Jiang F., Hearin A., Campbell D., Watson D., Padmanabhan N., 2014, MNRAS, 445, 1713
Vogelsberger M. et al., 2014, MNRAS, 444, 1518
Volonteri M., Natarajan P., Gültekin K., 2011, ApJ, 737, 50

This paper has been typeset from a TEX/LATEX file prepared by the author.